Effect of osmotic pressure on pore formation in lipid bilayers by the antimicrobial peptide magainin 2

Effect of Osmotic Pressure on Pore Formation in Lipid bilayers by the Antimicrobial Peptide Magainin 2

Md. Masum Billah,[1] Samiron Kumar Saha,[1, $] Md. Mamun Or Rashid,[1, #] Farzana Hossain,[2] and Masahito Yamazaki[1, 2, 3, *]

[1] *Integrated Bioscience Section, Graduate School of Science and Technology, Shizuoka University, Shizuoka 422-8529, Japan,* [2]*Nanomaterials Research Division, Research Institute of Electronics, Shizuoka University, Shizuoka 422-8529, Japan,* [3]*Department of Physics, Faculty of Science, Shizuoka University, Shizuoka 422-8529, Japan*

[$]Present address: Department of Physics, Pabna University of Science and Technology, Pabna-6600, Bangladesh

[#]Present address: Department of Pharmacy, Noakhali Science and Technology University, Noakhali-3814, Bangladesh

***Correspondence should be addressed to:**

Dr. Masahito Yamazaki

Nanomaterials Research Division, Research Institute of Electronics,

Shizuoka University, 836 Oya, Suruga-ku, Shizuoka 422-8529, Japan

Tel/Fax: 81-54-238-4741

E-mail: yamazaki.masahito@shizuoka.ac.jp

ABSTRACT

Osmotic pressure (Π) induces membrane tension in cells and lipid vesicles, which may affect the activity of antimicrobial peptides (AMPs) by an unknown mechanism. We recently quantitated the membrane tension of giant unilamellar vesicles (GUVs) due to Π under physiological conditions. Here, we applied this method to examine the effect of Π on the interaction of the AMP magainin 2 (Mag) with single GUVs. Under low Π values, Mag induced the formation of nanometer-scale pores, through which water-soluble fluorescent probe AF488 permeates across the membrane. The rate constant for Mag-induced pore formation (k_p) increased with increasing Π. It has been proposed that the membrane tension in the GUV inner leaflet (σ_{in}) caused by Mag binding to the outer leaflet plays a vital role in Mag-induced pore formation. During the interactions between Mag and GUVs under Π, the σ_{in} increases due to Π, thereby increasing k_p. The relationship between the k_p and the total σ_{in} due to Π and Mag agreed with that without Π. In contrast, Mag induced rupture of a subset of GUVs under higher Π. Using fluorescence microscopy with a high-speed camera, the GUV rupture process was revealed. First, a small micrometer-scale pore was observed in individual GUVs. Then, the pore radius increased within ~100 ms without changing the GUV diameter and concomitantly the thickness of the membrane at the pore rim increased, and finally the GUV transformed into a membrane aggregate. Based on these results, we discussed the effect of Π on Mag-induced damage of GUV membranes.

1. Introduction

When osmotic pressure (Π) is applied to cells and lipid vesicles, tension is produced in plasma membranes and lipid bilayers. This membrane tension affects the physiological function of membrane proteins and the physical properties of these membranes (1-3). The effects of Π on physical properties of lipid bilayers have been investigated using a suspension of large unilamellar vesicles (LUVs). The leakage of small water-soluble probes from the LUVs under Π has been estimated to elucidate the Π-induced pore formation in the LUV membranes (4,5). The Π-induced volume change of LUVs and changes in other physical properties have been examined using the LUV suspension method (many references cited in Ref. 6). Osmotic pressure affects not only the function of membrane proteins such as mechanosensitive ion channels but also that of lytic peptides (e.g., venom peptide such as mastoparan and melittin). These peptides can induce leakage of internal contents from eukaryotic cells. It was reported that osmotic pressure affects the interaction of lytic peptides with LUVs (7). However, it is difficult to obtain details about the elementary processes and mechanisms using the LUV suspension method. There are many LUV shapes in a suspension of LUVs, including nonspherical vesicles that change their shape upon the application of osmotic pressure (8,9). Thus, to investigate the effect of membrane tension due to osmotic pressure, it is necessary to select spherical LUVs. However, it is difficult to separate spherical LUVs from an ensemble of LUV shapes. In contrast, we are capable of observing the size and shape of giant unilamellar vesicles (GUVs) in a buffer using optical microscopy (10,11), and selecting only spherical GUVs for analysis of interactions with peptides and proteins. It has been demonstrated recently that the data using the GUVs provide more valuable information on Π-induced pore formation and leakage of internal contents (6,12,13).

Antimicrobial peptides (AMPs) have an activity to suppress the proliferation of and kill bacterial cells. Most AMPs attack the plasma membrane of bacterial cells and induce leakage of the internal contents, which is considered the main mechanism of their antimicrobial activities (14-16). The leakage of fluorescent probes from LUVs has been investigated using LUV suspensions to monitor AMP-induced damage to lipid bilayers (17-21). Generally, vesicle leakage occurs due to various mechanisms including pore formation, membrane fusion,

solubilization of membranes, and vesicle rupture (22). However, observation of interactions with individual LUVs is not possible; thus, it is very difficult to identify the underlying leakage mechanism. In contrast, observation of interactions between AMPs and individual GUVs permits identification of internal content leakage, structural changes, and physical properties, which provides direct information regarding the leakage mechanism (23). Statistical analysis of changes of the physical quantities of the examined single GUVs will enable acquisition of detailed information on elementary leakage processes such as the rate constant for pore formation, the rate constant for leakage, and the membrane permeability coefficient (23). Using a single GUV method, we can categorize the cause of substance-induced leakage as toroidal pore (e.g., magainin 2 (Mag)), channel-like pore (e.g., lysenin), vesicle rupture (or burst) (e.g., epigallocatechin gallate), or local rupture (e.g., lactoferricin B).

Using single GUVs, we examined the effect of membrane tension on the interaction of AMP Mag with lipid bilayers by applying membrane tension to single GUVs due to the pressure difference between the inside and the outside of a micropipette (i.e., the micropipette aspiration method) (24). During the interaction of Mag with a single GUV with membrane tension, the GUV is suddenly aspirated into the micropipette. It is interpreted that this aspiration of the GUV occurs because of GUV rupture triggered by Mag-induced pore formation in the GUV membrane. This is the same interpretation for the results of the tension-induced rupture of GUVs (25-28), where during the application of membrane tension to a GUV using the micropipette aspiration method we observe the sudden aspiration of the GUV into the micropipette. This result is interpreted as follows: first membrane tension induces a nanometer-scale pore in the GUV membrane, then membrane tension enlarges the radius of pore, resulting in rupture of GUV, and finally the GUV is rapidly aspirated into the micropipette due to the pressure difference between the inside and the outside of a micropipette (25-28). Statistical analysis of a large population of Mag-induced rupture of GUVs under membrane tension provides the rate constant for GUV rupture, which is almost the same as that for pore formation, because the GUVs are aspirated into the micropipette immediately after pore formation (24). The rate constant for GUV rupture increases with increasing membrane tension, indicating that the rate constant for Mag-induced pore formation increases with

increasing membrane tension. However, this method does not permit the direct observation of Mag-induced pore formation in the membrane owing to the rapid aspiration of the GUV into the micropipette, and we cannot obtain details on pore evolution because the GUV is aspirated immediately after pore formation.

In this study, to overcome this drawback of the micropipette aspiration method to apply membrane tension to GUVs, we used the osmotic pressure method to apply membrane tension to GUVs for the study of the effect of membrane tension on AMP-induced pore formation. So far, there has been no methods to estimate experimentally the membrane tension of the GUVs under Π. Recently we have developed a new experimental method to estimate accurately the membrane tension in spherical GUVs, and succeeded in measuring the values of membrane tension in GUVs under Π in water (6) and in a buffer containing 150 mM NaCl (which is similar to the physiological condition of human body) (12), which agree with their theoretical values. Later, other researchers also obtained the similar values of membrane tension of GUVs under Π using a different method (29). We can reasonably expect that the AMP-induced pore formation in the GUV membrane and the following evolution of the pore is observed using the osmotic pressure method. This is supported by the fact that large osmotic pressure itself does not induce rupture of GUVs but forms a transient pore with a life time of less than 100 ms (6). This fact is reasonably explained as follows: immediately after Π-induced pore formation the membrane tension greatly decreases because of rapid leakage of the internal solution from the GUV lumen to its outside due to the positive pressure in the GUV lumen according to Laplace's law, and thus, the pore closes rapidly owing to the large line tension of the pore, which is well supported by the theories (30,31). Moreover, in this study, we applied only small membrane tension to GUVs using Π which does not induce pore formation nor rupture of GUVs. Under this condition, we examined the effect of membrane tension due to Π on the interaction of Mag with single GUVs, focusing on Mag-induced pore formation. Various membrane tensions due to Π can be applied to GUVs using a method reported previously (12). To monitor the leakage of fluorescent probes from single GUVs, we used a low concentration (6 μM) of the water-soluble fluorescent probe Alexa Fluor 488 hydrazide (AF488), because it does not induce significant osmotic pressure. Under low Π values, we found that Mag induces AF488 leakage from GUVs without significantly changing the radius of the GUVs.

This result indicates that Mag induces formation of nanometer-scale pores that cannot be detected using optical microscopy (i.e., the diameter of the pore is less than 0.5 μm), which is the same phenomenon observed in the absence of Π (23). The rate constant for Mag-induced pore formation increased with increasing Π. In contrast, under higher Π, Mag induced rupture of GUVs to be converted to membrane aggregates in some GUVs. To elucidate the processes underlying the GUV rupture, we observed Mag-induced shape changes in GUVs using fluorescence microscopy with a high time resolution (with fluorescent probe-labeled lipids). Based on these data, we discuss the effect of Π on the interaction of Mag with single GUVs.

2. MATERIALS AND METHODS

2.1. Chemicals

Dioleoylphosphatidylcholine (DOPC), dioleoylphosphatidylglycerol (DOPG), and 1,2-dioleoyl-*sn*-glycero-3-phosphoethanolamine-N-(7-nitro-2-1,3-benzoxadiazole-4-yl) (18:1 NBD-PE; hereafter abbreviated NBD-PE) were purchased from Avanti Polar Lipids Inc. (Alabaster, AL, USA). AF488 was purchased from Invitrogen (Carlsbad, CA, USA). Bovine serum albumin (BSA) was purchased from FUJIFILM Wako Pure Chemical Co. (Osaka, Japan). Mag was synthesized by the FastMoc method using an Initiator+ Alstra (Biotage, Uppsala, Sweden) (32), and purification of Mag was performed using reverse phase HPLC and verified using mass spectroscopy.

2.2. Preparation and purification of GUVs

GUVs composed of DOPG/DOPC (4/6; molar ratio) (hereafter abbreviated DOPG/DOPC (4/6)-GUVs) containing the water-soluble fluorescent probe AF488 were prepared using the natural swelling method (12,33). We used GUVs containing AF488 in their lumen to evaluate Mag-induced leakage, and the experiment evaluating Mag-induced shape changes used GUVs composed of DOPG/DOPC/NBD-PE (39/60/1) (hereafter abbreviated DOPG/DOPC/NBD-PE-GUVs) not containing AF488. First, 200 μL of a 1.0 mM mixture of DOPG and DOPC (DOPG/DOPC = 4/6) or a mixture of DOPG, DOPC, and NBD-PE (DOPG/DOPC/NBD-PE = 39/60/1) in chloroform in a glass vial were dried under a gentle stream of nitrogen gas and subsequently in a

vacuum desiccator for more than 12 h. Next, 20 μL Milli-Q was placed on the dry film in the glass vial and the mixture was incubated at 45–47 °C for 7 min (pre-hydration). The pre-hydrated film was then incubated with 1.0 mL buffer A (10 mM PIPES, pH 7.0, 150 mM NaCl and 1 mM EGTA) containing 6.0 μM AF488 (for leakage experiments only) and 100 mM sucrose for 2 h at 37 °C, which produces a GUV suspension. The GUV lumen's osmolarity (C_{in}^0) was 388 mOsm/L. After centrifugation (14000 g × 20 min at 20 °C) of the GUV suspension, the GUVs in the resultant supernatant were purified by the membrane filtering method to remove smaller GUVs, LUVs, free AF488, and sucrose (33). Briefly, after the filtration of the GUV suspension through a Nuclepore polycarbonate membrane (10 μm pore size; Whatman, GE Healthcare, Ltd., Buckinghamshire, UK) in buffer A containing 93 mM glucose (388 mOsm/L) at a flow rate of 1 mL/min for 1 h, the unfiltered GUV suspension was collected as a purified GUV suspension. The osmolarity of the buffer using the filtration is the same as that of the GUV lumen.

2.3. Application of osmotic pressure to GUVs

To apply an osmotic pressure to GUVs and estimate its induced membrane tension, we used the same methods described previously (6,12). When GUVs with lumenal osmolarity of C_{in}^0 (mOsm/L) are transferred into a hypotonic solution with an osmolarity of C_{out} (mOsm/L), the osmotic pressure Π applied to the GUVs is equal to $RT\Delta C^0$, where $\Delta C^0 = C_{in}^0 - C_{out}$, R is the gas constant and T is the absolute temperature. Here, mOsm/L is the same as mM (mmol/L) or mol/m^3 (6). Under this condition, the radius of the GUV (its initial radius of r_0) increases by Δr_{eq} at equilibrium, and consequently a membrane tension at the swelling equilibrium (σ_{osm}) is produced in the GUV membrane. Based on the theory developed in our previous report (12), we can obtain the following equations for GUVs in a buffer containing a physiological ion concentration.

$$\sigma_{osm} = \frac{2K_{bil}\Delta C^0}{3C_{out}} \quad (1)$$

$$\frac{\Delta r_{eq}}{r_0} = \frac{\Delta C^0}{3C_{out}} \quad (2)$$

where K_{bil} is the elastic modulus of a lipid bilayer. For the DOPG/DOPC (4/6)-GUVs in buffer A containing ~100 mM glucose, the experimental values of σ_{osm}, and $\Delta r_{eq}/ r_0$ agree with the theoretical values obtained by Eqs. 1 and 2 (12).

2.4. Magainin 2-induced leakage of AF488 from single GUVs under osmotic pressure

The method described in section 2.3 was used to apply osmotic pressure. Briefly, a suspension of GUVs containing 6.0 μM AF488, purified according to section 2.2, was transferred into buffer A with a lower osmolarity compared with the GUV lumen (12) in a microchamber pre-coated with BSA (22). The single GUV method was used for the experiments evaluating interactions between Mag and single DOPG/DOPC (4/6)-GUVs (22,23). The interaction of Mag with single GUVs containing 6.0 μM AF488 was induced by the continuous addition of a Mag solution to the vicinity of a GUV by a micropipette (20-μm-diameter) whose tip was placed at a distance of 70 μm from the target GUV using a positive pressure of 30 Pa. Under this condition, the Mag concentration near the GUV was 78% of the Mag concentration in the micropipette (24). During interactions at 25 ± 1 °C, which was controlled by a thermo-controlled stage system, the shape and AF488 fluorescence intensity of the GUV were monitored using an inverted fluorescent phase-contrast microscope (IX-73, Olympus, Tokyo, Japan) with a digital CMOS camera (ORCA-Flash 4.0 V3, Hamamatsu Photonics K.K., Hamamatsu, Japan). To prevent AF488 photobleaching, two neutral density (ND) filters (a ND6 filter and a ND25 filter) were used to control the intensity of the incident light. The exposure time was 1.0 s. The intensity of AF488 fluorescence of the GUV lumen was analyzed using HCImage software (Hamamatsu Photonics K.K.). The detailed experimental procedure of the single GUV method was reported previously (22,24).

2.5. Magainin 2-induced shape changes in single GUVs under osmotic pressure

The method described in section 2.3 was used to apply osmotic pressure. DOPG/DOPC/NBD-PE-GUVs were prepared according to section 2.2. The method of investigating interactions between Mag and single GUVs was described in section 2.4. The NBD-PE fluorescence images and phase-contrast images of GUV shapes were monitored at 25 ± 1 °C using an inverted fluorescent phase-contrast microscope (IX-73) with an ORCA-Flash 4.0 V3 camera with an exposure time of 10 ms, and subsequently analyzed using HCImage software. To prevent photobleaching of NBD-PE, a neutral density (ND) 25 filter was used to control the intensity of the incident light.

2.6. Measurement of magainin 2-induced changes in GUV membrane area under osmotic pressure

Mag-induced changes in GUV area in the presence of osmotic pressure were measured using the micropipette method (24,34). A suspension of GUVs purified according to section 2.2 was transferred into buffer A with a lower osmolarity relative to the GUV lumen (12) in a microchamber pre-coated with BSA. The GUVs were observed at 25 ± 1 °C using an inverted differential interference contrast (DIC) microscope (IX-71, Olympus) with a CMOS camera (JCS-HR5UL, Olympus). We applied a slight aspiration pressure to individual GUVs in the solution using a micropipette α (10-μm-diameter) to hold the GUV at the micropipette's tip (which induces a membrane tension in the GUV of 0.5 mN/m) (24). The micropipette was coated with BSA and filled with buffer A of the same osmolarity as the buffer in the microchamber containing the GUVs. After the GUV was maintained under this condition for 2 min to eliminate the hidden-excess area of the GUV such as long, narrow tubes (references cited in Ref. 6), we applied a positive pressure of 30 Pa to another micropipette β (20-μm-diameter) whose tip was located ~40 μm from the GUV to continuously add a Mag solution from micropipette β to the vicinity of the GUV. The Mag solution had the same osmolarity as the buffer in the microchamber. The pressure in the micropipette was precisely controlled using a differential pressure transducer (22,24). This condition resulted in the Mag concentration near the GUV being 58% of the Mag concentration in micropipette β (24).

The changes in Mag-induced GUV membrane area is calculated as follows. Before exposure to Mag, the area of a GUV membrane is S_0. During the interaction with Mag, the area of the GUV (S) increases with time and reaches an equilibrium value (S_{eq}). The GUV area change, ΔS (= $S - S_0$), can be expressed by the fractional area change (δ), which is equal to $\Delta S/S_0$. If we assume the volume of the GUV changes during the interaction, then δ can be obtained as follows (35):

$$\delta = \frac{\Delta L d_p + D_V^2 - D_{V0}^2}{D_{V0}^2} \quad (3)$$

where ΔL is the change in projection length of the GUV inside the micropipette after interaction with Mag, D_V and D_{V0} are the diameter of the spherical region of the GUV outside micropipette α after and before interaction with Mag, respectively, and d_p is the inner diameter of micropipette α.

3. RESULTS AND DISCUSSIONS

3.1. Magainin 2-induced pore formation in single GUVs in the presence of osmotic pressure

To elucidate the effects of Π on Mag-induced pore formation, the interaction of Mag with single DOPG/DOPC (4/6)-GUVs containing 6.0 μM AF488 in buffer A in the presence of Π was investigated using the single GUV method (22,23). It is well known that large constant tension induces pore formation in GUVs (27,28). For DOPG/DOPC (4/6)-GUVs in buffer A (containing 150 mM NaCl) used in this report, no pore formation occurs at a tension of 3.0 mN/m or less (27). Hence, here we used relatively low osmotic pressures that induce membrane tensions of < 3.0 mN/m.

Initial experiments examined the interaction of 20 μM Mag with single GUVs (C_{in}^0 = 388 mOsm/L) in buffer A containing 88.0 mM glucose (C_{out} = 383 mOsm/L). An osmotic pressure (ΔC^0 = 5 mOsm/L) was then applied to the GUV, whose membrane tension was estimated to be 1.2 mN/m using Eq. 1. The parameters (C_{in}^0, C_{out}, and ΔC^0) are defined in section 2.3. Figure 1A shows a representative result. Before the interaction, a GUV image obtained using phase-contrast microscopy exhibited high contrast (Fig. 1A (1)), due to the difference in refractive index between the GUV lumen and its exterior, which is attributed to the differences in sucrose and glucose concentrations. An image of the same GUV obtained using fluorescence microscopy (Fig. 1A (2)) shows a high intensity of AF488 fluorescence in the GUV lumen at time t = 0. During the interaction between Mag and the GUV, the intensity of AF488 fluorescence in the GUV lumen (I) did not change for the first 192 s, and then decreased gradually to become almost zero at 284 s (Fig. 1A (2)). After the fluorescence intensity reached zero, a phase-contrast image of the same GUV (Fig.1A (3)) showed that the GUV shape and size did not change, while the phase contrast greatly decreased. As discussed previously (28,29), the decrease in I was due to membrane permeation of AF488 from the GUV lumen to its exterior through Mag-induced nanometer-scale pores in the GUV membrane and the decrease in phase contrast indicates the membrane permeation of sucrose from the GUV lumen through the same Mag-induced pores. Figure 1B shows a time course of changes in the normalized AF488 fluorescence intensity in the GUV lumen at time t, $I(t)/I(0)$ (i.e., the ratio of the I at interaction time t to the initial I at t = 0). Thus, the advent of decreases in I corresponds to the onset of membrane permeation of AF488, i.e., pore formation. When we performed the same experiments using 12 single GUVs

(the number of examined GUVs, n, was 12), we observed that the membrane permeation of AF488 from individual GUVs began at different times, indicating that pores were formed stochastically. As demonstrated previously (22,24), the rate constant for pore formation at its initial stage can be estimated by an analysis of the time course of the fraction of intact GUVs with no leakage of AF488 among all examined GUVs, $P_{\mathrm{intact}}(t)$. Theoretically, this phenomenon can be regarded as a two-state transition from the intact state to the initial pore state. Thus, P_{intact} can be expressed by a single exponential function as follows (22,24),

$$P_{\mathrm{intact}}(t) = \exp\{-k_{\mathrm{p}}(t - t_{\mathrm{eq}})\} \tag{4}$$

where k_{p} is the rate constant for the two-state transition, or the rate constant for Mag-induced nanometer-scale pore formation at its initial stage, and t_{eq} is a fitting parameter. The P_{intact} of GUVs under this condition (20 μM Mag and ΔC^0 = 5 mOsm/L) was well fitted by Eq. 4 (Fig. 1C), providing a k_{p} value of 5.9×10^{-3} s^{-1}. The value of k_{p} for this condition was $(8 \pm 2) \times 10^{-3}$ s^{-1} (the number of independent experiments, N, was 3). We performed the same experiment (interaction of 20 μM Mag with single GUVs) using GUVs under isotonic conditions (i.e., ΔC^0 = 0 mOsm/L), and found that k_{p} was $(4.5 \pm 1.5) \times 10^{-3}$ s^{-1} (N = 3). Hence, the k_{p} value increased with increasing ΔC^0, i.e., the osmotic pressure.

Next, we performed experiments examining the interaction of 20 μM Mag with single GUVs ($C_{\mathrm{in}}{}^0$ = 388 mOsm/L) in buffer A containing 81.0 mM of glucose (C_{out} = 376 mOsm/L). Under this condition, an osmotic pressure (ΔC^0 =12 mOsm/L) applied to the GUVs induces membrane tension of 2.6 mN/m in the GUVs (12). We obtained three types of results, which we name leakage without rupture, complete GUV rupture, and transient rupture. Figure 2A shows a representative result of "leakage without rupture" due to the formation of nanometer-scale pore in the GUV membrane, which is analogous to the result shown in Fig. 1. Figure 2D indicates that the starting time of the decrease in I is 111 s, which corresponds to the onset of membrane permeation of AF488, i.e., the onset of nanometer-scale pore formation. Figure 2B shows a representative result of complete rupture of a GUV. Before Mag exposure, a phase contrast image of a GUV exhibited high contrast (Fig. 2B (1)), and the corresponding fluorescence image at t = 0 (Fig. 2B (2)) showed high AF488 fluorescence intensity. During the interaction between Mag and the GUV, the AF488 fluorescence intensity in the GUV

lumen (I) decreased rapidly from the initial intensity I (0) at 20 s and reached 10% of I (0) at 24 s (Fig. 2B (2), 2E). After the intensity reached zero, we were unable to observe a phase-contrast image of the spherical GUV, rather, only a membrane aggregate was observed (Fig. 2B (3)). This result indicates that Mag induced complete rupture (or bursting) of the GUVs and consequently a rapid leakage of AF488 occurred, with the GUVs ultimately being reduced to membrane aggregates. This shape change, i.e., the complete rupture (or bursting) of GUVs, was observed in the interactions of single GUVs with the antimicrobial substance epigallocatechin gallate (36). Figure 2E shows a time course of change in $I(t)/I(0)$. The onset time of the decrease in I corresponds to the onset of the rupture of the GUV. In a few GUVs (~10% of all examined GUVs), another shape change was observed; where after the rapid leakage of AF488, a smaller, spherical GUV was observed (Fig. 2C). We termed this GUV shape change "transient rupture" based on the results shown in Fig. 4E (see the details in the section 3.2), although the similar shape change induced by AMP lactoferricin B was previously termed "local rupture" because of the AMP-induced decrease in radius of spherical GUVs (37). When the same experiments were performed using 15 single GUVs, we observed leakage without rupture in 7 GUVs, complete rupture in 6 GUVs, and transient rupture in 1 GUV. Figure 2F shows the time course of the fraction of intact GUVs with no AF488 leakage among all examined GUVs, $P_{\mathrm{intact}}(t)$. If we consider that the origin of complete rupture and transient rupture is Mag-induced nanometer-scale pore formation (see the details in the section 3.2 and the general discussion), we can regard both complete rupture and transient rupture as pore formation events. Thus, we can apply the theory of a two-state transition from the intact state to the initial pore state, which is expressed by Eq. 4. The P_{intact} of GUVs under this condition (20 μM Mag and ΔC^0 = 12 mOsm/L) was well fitted by Eq. 4 (Fig. 2F), providing a k_{p} value of $1.7 \times 10^{-2}\ \mathrm{s}^{-1}$. The k_{p} value for this condition was $(1.3 \pm 0.5) \times 10^{-2}\ \mathrm{s}^{-1}$ (N = 4). In Fig. 2F, we marked the data points corresponding to the leakage without rupture, complete rupture, and transient rupture using different colored symbols, which shows that there is no preferential distribution of any of the three observed effects along time. A similar result was observed in three additional repetitions of the same experiment. These results also support that the origin of complete rupture and transient rupture is Mag-induced

pore formation. Figure 3 shows the effect of Π on the rate constant of Mag-induced pore formation (k_p). It is clear that the k_p increases with increasing Π.

3.2. Process of the magainin 2-induced rupture of GUVs

To reveal the mechanism underlying Mag-induced GUV rupture, we attempted to observe the detailed processes of shape changes of the GUVs using NBD-PE fluorescence at a 10 ms time resolution. Since NBD-PE is incorporated in the GUV membrane, we can monitor shape changes of the GUV membrane during rupture using fluorescence microscopy. Figure 4A shows a representative shape change of a GUV during its complete rupture induced by Mag (the conditions were 20 μM Mag with a single GUV under an osmotic pressure due to ΔC^0 =12 mOsm/L, i.e., $C_{in}{}^0$ = 388 mOsm/L and C_{out} = 376 mOsm/L). At the beginning of the interaction, the GUV had a homogeneous fluorescence intensity in the membrane. At 20.020 s, a small spot of the GUV membrane, indicated by an arrow, exhibited decreased fluorescence intensity. The size of the spot of the membrane region with the absence of brightness increased with time and reached a maximum at 20.070 s (50 ms after the initial observation). Brochard-Wyart and colleagues reported the growth and closure of a pore induced by photochemical reaction-driven tension in a GUV using a similar method (38,39). According to them, the spot of the membrane region with the absence of brightness corresponds to a micrometer-scale pore (which can be observed using optical microscopy) produced in the GUV membrane. Therefore, the result shown in Fig. 4A indicates that Mag induced a micrometer-scale pore at 20.020 s and its size increased over time to 20.070 s (Fig. 4C), where the arc length of the spot of the membrane region with the absence of brightness is used as the pore size. After 20.070 s, the arc length increased and the fluorescent microscopic image ultimately showed that the GUV became a membrane aggregate (21.610 s of Fig. 4A (2)) and the corresponding phase contrast image shows an image of the aggregated membrane (Fig. 4A (3)). Before pore formation, the fluorescence intensity of NBD-PE was homogeneous throughout the GUV membrane. In contrast, after pore formation (notably after 20.040 s) the edge of the membrane contacting the pore exhibited a higher fluorescence intensity that increased with time. This result suggests that at the edge of the pore, the membrane folds together and becomes thicker.

Figure 4B shows another example of shape change during Mag-induced complete GUV rupture under the same conditions. At 17.250 s, the left rim of the GUV started to become irregular, and this rim irregularity increased with time. This indicates that micrometer-scale pore formation occurred at the back of the GUVs, thereby making it difficult to directly visualize the pore. After 17.290 s, the edge of the membrane contacting the pore exhibited an increased fluorescence intensity, which concomitantly increased with decreasing area of the GUV. The process of complete rupture of GUVs induced by Mag is similar to that induced by the epigallocatechin gallate (36).

In contrast, Fig. 4D shows that the phase contrast of a GUV under the same conditions (20 μM Mag and ΔC^0 = 12 mOsm/L) greatly decreased after 91 s interaction of Mag with the GUV without appearance of any micrometer-scale pores in the membrane and rupture of GUV. This membrane permeation of sucrose from the GUV lumen indicates that Mag induced pore formation in the GUV membrane, because such rapid membrane permeation does not occur without pore formation, and thus, this interaction belongs to the mode of "leakage without rupture" shown in Fig. 2A. Therefore, this result indicates that in the mode of "leakage without rupture" the pores are much too small to be observed and likely correspond to a nanometer-scale pore (Fig. 4D).

We also investigated the shape changes of the GUVs to reveal the mechanism underlying Mag-induced transient rupture of GUVs. Figure 4E shows a representative shape change during the Mag-induced transient rupture of the GUV under the same conditions (20 μM Mag and ΔC^0 =12 mOsm/L). At the beginning of the interaction, the GUV had a homogeneous fluorescence intensity in the membrane. At 58.450 s, a small spot of the GUV membrane (pointed by an arrow) exhibited a lower fluorescence intensity, and then the size of the spot of the membrane region with the absence of brightness, i.e., a micrometer-scale pore size, increased with time to reach a maximum, and then decreased with time until the micrometer-scale pore closed. Figure 4F (○) shows that the pore size (determined by the arc length of the spot of the membrane region with the absence of brightness) reached a maximum at 58.560 s (after 110 ms from the initial observation). The estimation of the pore size during its decrease from the maximum by the arc length is difficult because the shape of GUV in Fig. 4E is distorted from the spherical shape, and thus instead of the arc length we used the radius of the pore

determined by the half of the distance between both ends of the spot of the membrane region with the absence of brightness in the GUV membrane (36). Figure 4F (■) shows that the radius of the pore reached a maximum at 58.560 s, then decreased with time, and finally the micrometer-scale pore disappeared at 59.000 s. After that, the closed GUV appeared but its diameter decreased by 10 percent. This result indicates that Mag induces a micrometer-scale pore at 58.450 s and its radius increases with time by 58.560 s, and then it decreases with time until it closes completely (Fig. 4F). As shown in Fig. 4E, after formation of a micrometer-scale pore, the edge of the membrane contacting the pore did not exhibit a higher fluorescence intensity, which is different from the case of the complete rupture (Fig. 4A and 4B).

These results clearly indicate that in the Mag-induced complete rupture and transient rupture of GUVs, at the initial stage formation of a pore occurs in the GUV membrane and its radius is expanded, and finally the GUVs are converted into the aggregation of the membranes and a GUV with a smaller diameter, respectively. Thus, these results indicate that the complete rupture and transient rupture of GUVs are originated from pore formation in the GUV membrane.

3.3. Effect of osmotic pressure on magainin 2-induced area changes in GUVs

It is reported that the binding of Mag to a GUV increases its area (24). Here we examined the effect of Π on Mag-induced GUV area changes using the micropipette method. The method of applying Π to the GUVs is the same as that used in the section 3.1. First, we adopted the experimental conditions (of peptide concentration and osmotic pressure) that do not induce pore formation in most GUVs, because the pore formation induces rapid aspiration of the GUV into the micropipette and as a result we cannot measure the GUV area change. Thus, the interaction of 5.8 μM Mag with single GUVs in the presence of osmotic pressure due to ΔC^0 =12 mOsm/L was investigated. After starting interaction of Mag with a single GUV fixed at the tip of a micropipette in the presence of Π, the projection length of the GUV inside the micropipette increased (Fig. 5A). More quantitatively, the fractional area change of the GUV (δ) increased with time to reach a constant value within ~60 s (Fig. 5B), which can be considered an equilibrium value of δ (δ_{eq}). The time course of change in δ is

almost the same as that of the GUVs in the absence of Π (24). Previously, the binding of Mag to the outer leaflet of single GUVs under the same conditions was also investigated using fluorescence probe-labeled Mag (24): the binding occurs rapidly to reach its equilibrium in less than 50 s and the time course of the increase in Mag concentration in the GUV membrane is almost the same as the time course of change in δ. Therefore, the value of δ_{eq} is due to the equilibrium binding of Mag to the outer leaflet of the GUVs. Figure 5C shows the equilibrium value of the Mag-induced fractional area change of the GUVs (δ_{eq}) in the presence of various osmotic pressures. Under isotonic conditions (ΔC^0 = 0 mOsm/L), the mean value and standard error of δ_{eq} was 0.031 ± 0.001 (n = 42 in N = 3). Increased Π resulted in decreased δ_{eq} values: 0.027 ± 0.001 (n = 20 in N = 2) at ΔC^0 = 5 mOsm/L and 0.020 ± 0.001 (n = 36 in N = 3) at ΔC^0 = 12 mOsm/L.

Next, we investigated the interaction of 20 μM Mag with single GUVs in the presence of Π. Under isotonic conditions (ΔC^0 = 0 mOsm/L), δ_{eq} was 0.041 ± 0.001 (n = 18 in N = 2). However, in the presence of ΔC^0 =5 mOsm/L, most GUVs were aspirated into the micropipette due to pore formation in the GUV membrane before reaching an equilibrium value of δ, and thus, the value of δ_{eq} could not be obtained.

The effect of Π on Mag-induced area changes can be explained as follows. It is thought that Mag inserts deeply in the membrane interface as an α-helix (parallel with the membrane surface (40,41)) due to high membrane interfacial hydrophobicity (32,42). Since the α-helix can be considered a rigid cylinder, insertion of the α-helix deeply in the membrane interface results in the production of a steric repulsive force between the α-helix and lipid molecules (mainly their head groups). This interaction induces conformational changes of lipids, which increases the cross-sectional area of lipids under the peptide, thereby inducing an increase in the area of the outer leaflet (43). In GUVs under Π, stretching of the outer leaflet occurs before the interaction with Mag, and thus when Mag binds to the stretched outer leaflet, it is reasonably expected that the fractional area increases are smaller following Mag binding.

4. General Discussion

In this report, we succeeded in observing Mag-induced pore formation and its evolution in single GUVs under Π. Under low Π values, Mag induces membrane permeation of the water-soluble fluorescent probe AF488 from the GUVs without their rupture, indicating that Mag causes the formation of nanometer-scale pores through which AF488 permeates across the membrane but cannot be observed using optical microscopy. In contrast, under higher Π, in some GUVs Mag causes the formation of nanometer-scale pores, which is analogous to the result obtained under low Π values, but in other GUVs Mag induces complete rupture and transient rupture of GUVs, which are originated from the Mag-induced pore formation. It is noted that in all cases the values of Π were too small to induce pore formation in the GUV membrane, and thus, the Π is used to induce small membrane tension. The rate constant of Mag-induced pore formation (k_p) increased with increasing osmotic pressure. As described in the Introduction, when we examined the effect of membrane tension on Mag-induced pore formation using the micropipette aspiration method, we observed the Mag-induced aspiration of GUVs into the micropipette and could not observe pore formation directly (24). In this report, using Π, we succeeded in observing Mag-induced pore formation under a membrane tension directly for the first time and revealed that the rate constant of Mag-induced pore formation increases with increasing membrane tension.

Recently, we proposed that during the interaction between Mag and GUVs, Mag binds to the membrane interface of only the outer leaflet (i.e., the asymmetric binding of Mag), resulting in stretching of the inner leaflet of the GUVs and the membrane tension in the inner leaflet (σ_{in}), which play a vital role in Mag-induced pore formation (24,44). In our previous report (24), we demonstrated using the micropipette aspiration method that Mag binds to only the outer leaflet in the presence of membrane tension of 3.0 mN/m, which is larger than the Π-induced membrane tension used in this report, based on the result that the fluorescence intensity of a GUV membrane due to fluorescent probe-labeled Mag does not exhibit a two-step increase. This conclusion is supported by the result of another AMP (e.g., PGLa) which binds to the lipid bilayer symmetrically (i.e., both the outer leaflet and the inner leaflet) that the fluorescence intensity of a GUV membrane due to fluorescent probe-labeled PGLa exhibits a two-step increase before pore formation under similar experimental conditions (but under the membrane tension of 0.5 mN/m) (45). These results indicate that in the presence of membrane

tension due to Π Mag binds to the membrane interface of only the outer leaflet. On the other hand, the binding of Mag to the outer leaflet may affect the lipid packing of the outer leaflet (43,46), which may also play a role in Mag-induced pore formation. According to the theory of asymmetric peptide binding at the membrane interface of the outer leaflet (43), the inner leaflet is stretched while the pure lipid region of the outer leaflet is compressed, indicating that the packing of lipids increases in the outer leaflet (43). The binding of peptides to the membrane interface may induce local deformation of lipid regions near the bound peptides (46). In this report, we found that stretching of the bilayer due to osmotic pressure increases the rate constant of Mag-induced pore formation. The presence of Π increases the stretching of both monolayers, which further stretches the inner leaflet while decreasing the compression of the pure lipid region as well as local deformation of the lipid region near the bound peptides in the outer leaflet. Therefore, this finding supports the proposed mechanism of Mag-induced pore formation (24,44).

Here, we quantitatively analyzed the effect of Π on Mag-induced pore formation based on our model (24,44). Under this condition, two kinds of membrane tension are induced in the inner leaflet of a GUV. One is the tension due to Π (σ_{in} (Π)) and the other is the tension due to the binding of Mag in the outer leaflet (σ_{in} (Mag)). If we assume the additivity of the two tensions, the total tension in the inner leaflet (σ_{in} (total)) equals the sum of σ_{in} (Π) and σ_{in} (Mag) (i.e., σ_{in} (total) = σ_{in} (Π) + σ_{in} (Mag)) (Fig. 6A). Previously we examined the effect of Π on the constant tension-induced rupture of GUVs (6,12). We demonstrated that membrane tension in the lipid bilayer due to Π (σ_{bil} (Π)) and that generated due to the aspiration of the GUV by a micropipette (i.e., an external force) (σ_{bil} (ex)) contribute the total tension in the lipid bilayer equivalently and the additivity of two kinds of tension holds (i.e., σ_{bil} (total) = σ_{bil} (Π) + σ_{bil} (ex)). Based on this result, we can reasonably infer that for the interaction of Mag with a GUV under Π the additivity of the two tensions, σ_{in} (Π) and σ_{in} (Mag), holds in the inner leaflet, and hence, σ_{in} (total) = σ_{in} (Π) + σ_{in} (Mag). First, we estimate the σ_{in} (Π) values numerically. We can use the reported values for the membrane tension in a lipid bilayer induced by osmotic pressure (σ_{bil} (Π)): 1.2 mN/m for ΔC^0 = 5 mOsm/L and 2.6 mN/m for ΔC^0 = 12 mOsm/L (12). Since the membrane tension in the inner leaflet due to osmotic pressure (σ_{in} (Π)) can be estimated as 50% of σ_{bil} (Π): we estimated σ_{in} (Π) as 0.6

mN/m for ΔC^0 = 5 mOsm/L and 1.3 mN/m for ΔC^0 = 12 mOsm/L. Next, we estimate the σ_{in} (Mag) values numerically. The σ_{in} (Mag) can be estimated by (K_{bil}/2) δ_{eq} because Mag is located only in the outer leaflet before pore formation (24), where K_{bil} is the elastic modulus of DOPG/DOPC (4/6) bilayer (K_{bil} = 141 mN/m under the same conditions used in this report (24)). As the results in Fig. 5 indicates, the osmotic pressure decreases the Mag-induced fractional area change of the GUV membrane at the binding equilibrium, δ_{eq}. Under an osmotic pressure due to ΔC^0 = 5 mOsm/L and 12 mOsm/L, the δ_{eq} due to the interaction with 5.8 μM Mag decreases by 13% and 35% of δ_{eq} in the absence of Π, respectively (i.e., δ_{eq} (ΔC^0)/δ_{eq} (0) = 0.87 and 0.65 for ΔC^0 = 5 mOsm/L and 12 mOsm/L, respectively, where δ_{eq} (ΔC^0) and δ_{eq} (0) are the equilibrium values of the fractional GUV area change in the presence and absence of Π, respectively) (Table 1A). In this report we determined that δ_{eq} = 0.041 for 20 μM Mag-induced area changes in GUVs under isotonic conditions. If we assume the effect of Π on δ_{eq} for the interaction of 20 μM Mag is the same as that for 5.8 μM Mag, we can estimate the δ_{eq} values of GUVs in the interaction of 20 μM Mag under Π using the same values of δ_{eq} (ΔC^0)/δ_{eq} (0) described above: δ_{eq} = 0.036 and 0.027 for ΔC^0 = 5 mOsm/L and 12 mOsm/L, respectively (Table 1B). Based on these values, we estimated the σ_{in} (Mag) values in the interaction of 20 μM Mag: 2.5 mN/m and 1.9 mN/m for ΔC^0 = 5 mOsm/L and 12 mOsm/L, respectively. Therefore, σ_{in} (total) = σ_{in} (Π) + σ_{in} (Mag) = 0.6 + 2.5 = 3.1 mN/m for ΔC^0 = 5 mOsm/L. This tension can induce a rate constant for pore formation of 1.1×10^{-2} s^{-1} (24), which is similar to the experimental value. Similarly, we obtained σ_{in} (total) for ΔC^0 = 12 mOsm/L: 1.3 + 1.9 = 3.2 mN/m (Table 1B). The relationship between σ_{in} (total) and k_p is plotted in Fig. 6B, showing that the k_p increases with an increase in σ_{in} (total). We compared this relationship with that of Mag in the absence of Π (24). The two datasets are almost superimposed, indicating that the value of σ_{in} (total) determines the rate constant of pore formation. Therefore, this result supports the above theory on the effect of Π on Mag-induced pore formation.

Based on our calculations, we can predict the rate constant for Mag-induced pore formation in single GUVs in the presence of Π. For the interaction of 5.8 μM Mag with single GUVs under an osmotic pressure due to ΔC^0 = 12 mOsm/L, δ_{eq} was 0.020, and thus, σ_{in} (Mag) = (K_{bil}/2) δ_{eq} = 1.4 mN/m. Therefore, σ_{in} (total) =

1.3 + 1.4 = 2.7 mN/m (Table 1A). To measure the rate constant (k_p) for Mag-induced pore formation, σ_{in} (total) should be greater than or equal to 2.9 mN/m (corresponding to 20 μM Mag and higher). This is the reason why we did not observe significant pore formation when we use this low Mag concentration. This prediction agrees with the experimental result.

As described in the introduction, it is considered that the tension-induced pore formation is the origin of the rupture of GUV, and thus here we can regard the constant tension-induced rupture of GUVs as the constant-tension-induced pore formation. Here, it is worth comparing the effects of Π on constant tension-induced pore formation and that on Mag-induced pore formation. In both cases, Π is used to induce small membrane tension in the lipid bilayer. When we apply a constant tension to a GUV under Π using the micropipette aspiration (6), σ_{bil} (total) can be expressed by the sum of σ_{bil} (Π) and σ_{bil} (ex), as described above. We obtained the experimental result that the rate constant of constant tension-induced rupture of GUV, i.e., the rate constant of pore formation in the GUV membrane, increases with σ_{bil} (total) (6). We can explain this fact by the standard theory of tension-induced pore formation (27,28,47-49). In the lipid bilayers at the liquid-crystalline phase, the fluctuation of lipid molecules is large due to thermal force, and thus, the lipid density at local regions is also fluctuated. A nanometer-size region with a lower lipid density is called a prepore. The formation of a prepore elevates the free energy of the membrane because it has a rim with an excess free energy per length, i.e., the line tension Γ, and thus the prepore closes rapidly. There are several models of prepores (47-53). Here we adopt a hydrophilic prepore whose wall is composed of hydrophilic segments of lipids of the curved monolayer. The free energy of a prepore with radius r in a stretched lipid bilayer, $U(r)$, can be described when the electrostatic interaction due to the surface charges of the lipid membrane is taken into account (28,54):

$$U(r) = 2\pi r\Gamma - \pi(\sigma + B)r^2 + U_0 \qquad (5)$$

where σ denotes the total membrane tension in the lipid bilayer of the GUV, B is a parameter representing the electrostatic interaction, and U_0 is a term that does not depend on σ. The maximum of $U(r)$, U_a, is the energy barrier of pore formation or the activation energy of the pore formation:

$$U_a = U_0 + \pi\Gamma^2/(\sigma + B)\cdot \qquad (6)$$

Thermal force induces the fluctuation of the prepore radius, and if the radius reaches a critical value, r_c, at which $U(r_c) = U_a$, pore formation occurs. Thus, the rate constant of pore formation increases with an increase in total tension because U_a decreases with the total tension. With an increase in Π, σ_{bil} (Π) increases, and thus, the total membrane tension increases. Therefore, this theory explains reasonably the effect of Π on the rate constant of constant tension-induced rupture of GUVs. On the other hand, in the interaction of Mag with a GUV under Π, the binding of Mag in the outer leaflet induces the stretching of the inner leaflet, producing σ_{in} (Mag) in the inner leaflet, and thus, σ_{in} (total) can be expressed by the sum of σ_{in} (Π) and σ_{in} (Mag) (i.e., σ_{in} (total) = σ_{in} (Π) + σ_{in} (Mag)) (Fig. 6A). Here, we define that σ is positive when a lipid leaflet is stretched. σ_{in} (Mag) > 0 and σ_{in} (Π) > 0, and thus, in the presence of Π, σ_{in} (total) increases by σ_{in} (Π). In the outer leaflet of the GUV composed of the peptide-lipid complex and the pure lipid region, based on the theory of the asymmetric distribution of peptides (43), the pure lipid region of the outer leaflet is compressed and the membrane tension in the outer leaflet (σ_{out} (Mag)) has the same magnitude as σ_{in} (Mag) with an opposite direction (i.e., σ_{out} (Mag) = $-\sigma_{in}$ (Mag)). This is supported by the experimental result that no flip-flop of lipids occurs in the interaction of Mag with single GUVs before pore formation (in this case the flip-flop of lipids occurs after pore formation) (44). It is reported that the rate constant of flip-flop of lipids increases in a stretched membrane because the rate of prepore formation increases with membrane tension (12). In the interaction of Mag with single GUVs, the rate of prepore formation increases in the stretched inner leaflet of the GUV, but in the outer leaflet, the membrane is compressed and thus the prepore formation is suppressed, and as a result, the flip-flop of lipids across the lipid bilayer does not occur significantly. The total tension in the outer leaflet (σ_{out} (total)) equals to (σ_{out} (Mag) + σ_{out} (Π)) and its direction is opposite to σ_{in} (total) (i.e., the compression in the outer leaflet) if $|\sigma_{out}$ (Mag)| > σ_{out} (Π) because σ_{out} (Mag) < 0. This condition is satisfied in all experiments (Table 1), and thus, we can reasonably infer that the outer leaflets of all GUVs used in this report are compressed. In the stretched inner leaflet, the σ_{in} (total) elevates the rate constant of pore formation. The free energy of a prepore with radius r in a stretched lipid monolayer can be described by an equation similar to Eq. 5 although the prepore exists only in the inner leaflet and has a little different structure from the prepore in the lipid bilayer (44). Thus, the rate

constant of pore formation in the inner leaflet increases with an increase in σ_{in} (total) because U_a decreases with σ_{in} (total). Immediately after pore formation occurs in the inner leaflet, pore formation occurs in the lipid bilayer, and thus, the rate constant of pore formation in the GUV membrane equals to that in the inner leaflet (24). In conclusion, one of the main differences between the effects of Π on constant tension-induced rupture of GUVs and that on Mag-induced pore formation is the region of stretching of the membrane, i.e., the lipid bilayer for the constant tension-induced rupture of GUVs and the inner monolayer for Mag-induced pore formation.

In our previous report, we demonstrated that Mag-induced leakage of internal contents has two stages; initially, rapid leakage occurs, and then, the rate of leakage decreases with time to reach a steady value (55). During the initial stage, large fluorescent probes such as Texas-red dextran 40K (Stokes-Einstein radius, r_{SE}: 5.0 nm) and FITC-BSA (r_{SE} = 3.6 nm) can permeate the Mag-induced pores. However, we cannot directly observe the initial pore using optical microscopy, indicating that the pore is not sufficiently large for observation using optical microscopy, i.e., the nanometer-scale pore. It is considered that the Mag-induced pore is a toroidal pore in the initial state and in the steady state (18,44,56), and thus, if the GUV membrane is stretched due to Π when Mag induces pore formation, the size of the initial pore may become larger than that in the absence of Π, because the size of toroidal pore can change (55). This prediction is supported by the results in this report that in the presence of higher Π, a small micrometer-scale pore that can be observed using fluorescence microscopy (i.e., the diameter of the pore is larger than 0.5 μm) is formed in a GUV membrane, the pore size then increases with time in some GUVs. These GUVs are ultimately converted to a small aggregate of lipid membranes and Mag (i.e., the complete rupture of GUV). At present, we do not have a definitive mechanism for the complete rupture of GUVs. Generally, under Π, immediately after formation of a pore in the membrane, a rapid flow of solution from the GUV lumen to its exterior (i.e., efflux) occurs due to the positive pressure in the GUV lumen according to Laplace's law (57), which decreases membrane tension, and as a result, the pore rapidly closes due to a large line tension of the pore rim so that a micrometer-scale pore is not observable (6). In this study, we found that in most completely ruptured and transiently ruptured GUVs, initial pore formation occurs at the backside of the GUV near the BSA-coated glass surface. In this case, the resistance to the efflux is enhanced

due to the presence of the obstacle of the flow (i.e., the glass surface), thereby maintaining membrane tension for a period of time. Moreover, after pore formation, Mag in the outer leaflet diffuses along the membrane interface to the wall of the (toroidal) pore and thus Mag locates at the wall of a pore (55), which decreases the line tension of the pore rim (Fig. 7B). Therefore, the remaining membrane tension and the small line tension of the pore rim would increase the pore radius to produce a micrometer-scale pore (Fig. 7C), which agrees with the experimental results. We can estimate the maximum radius of the pore under this condition as follows. Under Π, the GUV membrane is stretched and at equilibrium the fractional area change of the GUV membrane reaches δ_{eq} (Π). When a pore is formed in a stretched membrane, the radius of the pore increases as the area of the GUV membrane decreases, i.e., its stretching decreases. If we do not consider the closure of the pore due to the line tension of the rim of the pore, the maximum radius of the pore is reached when the GUV area decreases to its initial value at the tension-free state (i.e., the state prior to the application of Π). When the area of the pore equals the increment in GUV area due to osmotic pressure ($\Delta A = 4\pi r_0^2 \delta_{eq}$ (Π), where r_0 is the initial radius of the GUV), the stretching of the GUV membrane becomes 0. Thus, this pore corresponds to the largest pore when we only consider the theory of membrane elasticity. Here we show an example of the estimation of their numerical values based on the experimental results. In the case of ΔC^0 = 12 mOsm/L, δ_{eq} (Π) = 0.022 (12). If r_0 is 15 μm, the increase in GUV area due to Π, ΔA, is $4\pi r_0^2 \times 0.022$, which becomes the area of the largest pore (πR_{pore}^2, where R_{pore} is the maximum radius of the pore) and hence, $R_{pore} = 0.30 r_0$ = 4.5 μm. This indicates that the maximum radius of the pore (R_{pore}) is approximately 30% of the initial radius of the GUV (r_0). If the pore radius increases above its maximum, the GUV membrane is laterally compressed and an opposing tension to decrease the pore radius is produced, and thus, the pore radius cannot exceed the maximal value. This prediction does not agree with the experimental results on the complete rupture of GUVs. The fluorescence microscopy images of complete rupture of GUVs (e.g., Figs. 4A and 4B) indicate that the edge of the membrane contacting the pore exhibits a higher NBD-PE fluorescence intensity, which increases with time. This result suggests that folding of membranes occurs at the pore edge (Fig. 7D), which may inhibit the closure of micrometer-scale pores. We infer that the main factors for membrane folding are the low bending modulus of lipid bilayers in the

liquid-crystalline phase (i.e., membranes can bend easily) and the strong electrostatic attraction between positively charged Mag bound to the GUV membrane with the neighboring negatively charged lipid bilayers. The flow of the solution from the GUV lumen under the resistance may help the folding of the membrane at the pore edge. Finally, the diameter of the pore increases further with time to form a small aggregate of lipid membranes (Fig. 7E). A similar folding of membrane occurs in antimicrobial substance, epigallocatechin gallate (EGCg)-induced complete rupture of electrically neutral PC-GUVs (36); a micrometer-scale pore is initially formed in GUVs and the phase contrast of the edge of the pore increases with time. This indicates the folding of the membrane at the edge of the pore. Then, the diameter of the GUV decreases with time to form a compact, small aggregate of lipid membranes and the catechin (36). In this case, the strong attractive force between EGCg bound with a GUV membrane and a region of the neighboring GUV membrane is thought to cause folding of the lipid bilayers at the pore edge. In contrast, in the transient rupture of GUVs, the edge of the membrane contacting the micrometer-scale pore did not exhibit a higher fluorescence intensity (Fig. 4E), indicating that the folding of membrane does not occur at the pore edge (Fig. 7D′). Under this situation, the line tension of the micrometer-scale pore is not small, and thus, the pore closes rapidly to form a spherical GUV (Fig. 7E′).

It is reported that some AMPs and antimicrobial substances induce complete rupture of GUVs (36,58) and local rupture of GUVs (37,59). The antimicrobial substance, EGCg-induced rupture of PC-GUVs is described above. Some of the results of AMP-induced rupture and local rupture of GUVs were interpreted by the carpet model (60), where the AMPs interact with lipid bilayers as a kind of “detergent” molecule and solubilize the membrane, but the detailed mechanism is still unknown. The results in this report indicate that the AMPs which form toroidal pores in lipid bilayers (e.g., Mag) can induce rupture and local rupture of GUVs under a special condition (e.g., under osmotic pressure).

We can reasonably infer that the Mag-induced complete rupture of GUVs under a higher osmotic pressure (in this report) and the Mag-induced aspiration of GUVs held at the tip of micropipette (inducing a small tension to the GUV membrane) (24) occur by the same mechanism because membrane tension increases the size of Mag-induced pore in the GUV membrane and consequently induces the rupture of GUVs (in the latter case,

resulting in the aspiration of GUVs). This mechanism can be applicable only to the toroidal pore, but not to the channel-like pore (e.g., lysenin (23)) based on the following inference. The toroidal pore is composed of peptides and lipid monolayers, and the interaction between the peptides in the pore is small (18,44,56). Thus, it is easier to change the size of pore by membrane tension. In contrast, the channel-like pore is composed of oligomers of peptides/proteins with strong interaction between them, and thus, membrane tension cannot change the size of such pores.

There are various modes of interaction of AMPs with single GUVs. The type A AMPs induce membrane permeabilization in GUVs due to pore formation (e.g., Mag, transportan 10 (TP10) (23)) and local rupture (e.g., lactoferricin B (LfcinB) (37)). The type B AMPs enter the GUV lumen without membrane permeabilization (e.g., LfcinB (4-9)). Even in the type A, the relationship between the location of peptides and the pore formation depends on peptides and lipid compositions. Mag locates only in the outer leaflet before pore formation (i.e., asymmetric binding (43)) and after pore formation Mag translocates across the lipid bilayer by diffusing through the pore (24), whereas TP10 translocates across the lipid bilayer to reach the symmetric binding (i.e., same peptide concentration in both the outer and the inner leaflets) without membrane permeation of dyes, and then pore formation occurs. However, when TP10 interacts with GUVs containing high concentration of cholesterol, its behavior is completely the same as that of Mag (i.e., the asymmetric binding induces pore formation) (61). Some models have been proposed for the translocation of peptides across lipid bilayers without membrane permeation of dyes, and we also proposed a prepore model where peptides translocates across the lipid bilayer through a prepore (61). According to this model, the translocation of peptides across the lipid bilayer depends on the structure of peptides and also on the physical properties of lipid bilayers. Further studies are required to elucidate the mechanism of the translocation of peptides without pore formation.

It is valuable to compare the results of the effect of Π on peptide-induced pore formation obtained using the single GUV method in this report with the results obtained using the LUV suspension method (7). Polozov et al. found that the rate of leakage of fluorescent probes induced by a lytic peptide belonging to class L amphipathic peptides (18L) increases with Π (7). However, the LUV suspension method cannot yield data on

the elementary processes of leakage (22); thus, such experiments cannot determine the rate constant for pore formation and its dependence on Π. The results using the single GUV method reveal that at low Π fluorescent probe leakage occurs through Mag-induced nanometer-scale pores and at higher Π the leakage occurs not only by the nanometer-scale pores but also by Mag-induced complete rupture and transient rupture of GUVs; however, the LUV suspension method cannot provide such information because it is difficult to identify the cause of fluorescent probe leakage from the LUVs. Moreover, using the LUV suspension method it is not possible to experimentally determine membrane tension due to Π, as well as the details of constant tension-induced pore formation in vesicles. In this report, we examined the effect of Π on Mag-induced pore formation using the single GUV method in the context of detailed knowledge of membrane tension due to Π (6,12) and the effect of constant tension on the GUVs (27,28). Therefore, we succeeded in obtaining direct information on the effect of Π on peptide-induced leakage using the single GUV method.

Finally, we consider the physiological implications of the effects of membrane tension and Π on the AMPs-induced pore formation. Bacterial plasma membrane is prone to experience various membrane tensions. For example, Gram-negative bacterial cells exist in different stages in the cell cycle such as division and septation. We found that the rate of LfcinB-induced leakage of fluorescent probe from the cytoplasm of *E. coli* cells greatly depends on their stage in the cell cycle, and especially this rate from septating cells is much larger than that from nonseptating cells, indicating that the rate of LfcinB-induced pore formation or the damage in the plasma membrane of septating cells is larger than that of nonseptating cells (37). We have a hypothesis that in the septating cells, the Z-ring induces a large deformation of the plasma membrane, inducing a large membrane tension in it, which increases the rate of LfcinB-induced pore formation. Another example is that various values of Π are applied to bacterial cells if the environment of the cells changes, which induces membrane tension in their plasma membrane. This may affect the susceptibility to the attack by AMPs. It is important to investigate the effect of membrane tension and Π on the activity of AMPs against live bacterial cells near future.

5. Conclusion

In this report, we investigated the effect of Π on the interaction of Mag with single GUVs, based on the quantitative estimation on Π-induced membrane tension in GUVs in a buffer containing 150 mM NaCl (which is similar to the physiological condition of human body) (12). We succeeded in observing Mag-induced pore formation and its evolution in single GUVs under Π. Under low Π values, Mag induces the formation of nanometer-scale pores, through which AF488 permeates across the membrane but cannot be observed using optical microscopy. In contrast, under higher Π, in some GUVs Mag causes the formation of nanometer-scale pores, but in others Mag induces complete rupture and transient rupture of GUVs, which are originated from the Mag-induced nanometer-scale pore formation. At present, we have a hypothesis on the evolution of the Mag-induced nanometer-scale pore to the complete rupture and the transient rupture of a GUV and its mechanism as follows. In the Mag-induced pore, the line tension of the pore rim is small due to the presence of Mag at the pore rim, which stabilizes the toroidal pore, and if a large membrane tension due to Π remains after pore formation, it increases the pore radius to produce a micrometer-scale pore which can be observable using optical microscopy. In the case of complete rupture, the folding of membranes occurs at the micrometer-scale pore rim (demonstrated by the experimental results), which may further enlarge the micrometer-scale pore to induce a small aggregate of lipid membranes. In the case of transient rupture, the folding of membrane does not occur at the pore rim, and thus, the pore closes due to the line tension of the pore rim. These results provide the first, direct evidence of AMP-induced pore formation, complete rupture, and transient rupture (or local rupture) of GUVs with membrane tension. It is reported that some AMPs and antimicrobial substances induce complete rupture and local rupture of GUVs. The results in this report clearly indicate that the AMP-induced complete rupture and transient rupture (or local rupture) of GUVs under a special condition can be originated from AMP-induced pore formation.

The rate constant for Mag-induced pore formation (k_p) increases with increasing Π. This result can be explained by the increase in membrane tension in the inner leaflet of a GUV due to Π. The total tension of the inner leaflet, σ_{in} (total), when GUVs under Π interact with Mag, is the sum of σ_{in} due to the binding of Mag (σ_{in} (Mag)) and σ_{in} due to Π (σ_{in} (Π)). By the numerical estimation of these values, we estimated the values of σ_{in}

(total) and obtained the relationship between σ_{in} (total) and k_p, showing that the k_p increases with an increase in σ_{in} (total). This relationship is almost the same as that of Mag in the absence of Π. This result demonstrates that the above theory of the effect of Π on Mag-induced pore formation is valid.

These results clearly demonstrate that the single GUV method can directly reveal the effect of Π on Mag-induced pore formation in lipid bilayers. The experimental method developed in this report will be used to investigate the effect of Π on other AMPs-induced pore formation in lipid bilayers and on the interaction of peptides/proteins and membrane active substances with lipid bilayers. It is reported that in bacterial cells membrane tension and Π greatly affect the AMPs-induced pore formation in their plasma membrane and concomitant leakage of internal contents, which is the main cause of AMPs' bactericidal activity. Therefore, it is important to investigate the effects of membrane tension and Π on the AMP-induced pore formation in GUV membranes using the method developed in this report and also their effects on the action of AMPs against live bacterial cells.

Conflicts of interest: There are no conflicts to declare.

ACKNOWLEDGMENTS:

This work was supported by Grants-in-Aid for Scientific Research (B) (No. 19H03193) from the Japan Society for the Promotion of Science (JSPS) to M.Y., as well as by the Cooperative Research Project of Research Center for Biomedical Engineering.

References

1. F, Sachs, *Physiology*, 2010, **25**, 50-56.
2. S. I. Sukharev, P. Blount, B. Martinac, F. R. Blattner and C. A. Kung, *Nature*, 1994, 368, 265-268.
3. N. Levina, S. Totemeyer, N. R. Stokes, P. Louis, M. A. Jones and I. R. Booth, *EMBO J.*, 1999, **18**, 1730-1737.
4. C. Taupin, M. Dvolaitzky and C. Sauterey, *Biochemistry*, 1975**, 14**, 4771-4775.
5. A. Ertel, A. G. Marrangoni, J. Marsh, F. R. Hallert and J. Wood, *Biophys. J.*, 1993, **64**, 426-434.

6. S. U. A. Shibly, C. Ghatak, M. A. S. Karal, M. Moniruzzaman and M. Yamazaki, *Biophys. J.*, 2016, **111**, 2190-2201.
7. I. V. Polozov, G. M. Anantharamaiah, J. P. Segrest and R. M. Epand, *Biophys. J.*, 2001, **81**, 949-959.
8. B. L.-S. Mui, P. R. Cullis, E. A. Evans and T. D. Madden, *Biophys. J.*, 1993. **64**, 443-453.
9. H. Hotani, *J. Mol. Biol.*, 1984, **178**, 113-120.
10. K. Olbrich, W. Rawicz, D. Needham and E. Evans, *Biophys. J.*, 2000, **79**, 321-327.
11. J. C. S. Ho, R. Padmini, B. Liedberg and A. N. Parikh, *Langmuir*, 2016, **32**, 2151-2163.
12. S. K. Saha, S. U. A. Shibly and M. Yamazaki, *J. Phys. Chem. B*., 2020, **124**, 5588-5599.
13. W.-C. Su, D. L. Gettel, M. Chabanon, P. Rangamani and A. N. Parikh, *J. Amer. Chem. Soc*., 2018, **140**, 691-699.
14. M. Zasloff, *Nature*, 2002, **415**, 389-395.
15. M. N. Melo, R. Ferre and A. R. B. Castanho, *Nat. Rev. Microbiol.*, 2009, **8**, 1-5.
16. K. Matsuzaki, Ed., *Antimicrobial Peptides: Basic for Clinical Application*, Springer Nature, Singapore, 2019.
17. K. Matsuzaki, K. Murase, N. Fujii and K. Miyajima, *Biochemistry*, 1995, **34**, 6521-6526.
18. K. Matsuzaki, O. Murase, N. Fujii and K. Miyajima, *Biochemistry*, 1996, **35**, 11361-11368.
19. S. M. Gregory, A. Pokorny, P. F. F. Almeida, *Biophys. J.*, 2009, **96**, 116-131.
20. O. Aguilera, H. Ostolaza, L. M. Quirós and J. F. Fierro, *FEBS Lett*., 1999, **462**, 273-277.
21. W. Jing, J. S. Svendsen and H. J. Vogel, *Biochem. Cell Biol*., 2006, **84**, 312-326.
22. M. Yamazaki, *Adv. Planar Lipid Bilayers Liposomes*, 2008, **7**, 121-142.
23. M. Z. Islam, J. M. Alam, Y. Tamba, M. A. S. Karal and M. Yamazaki, *Phys. Chem. Chem. Phys*., 2014, **16**, 15752-15767.
24. M. A. S. Karal, J. M. Alam, T. Takahashi, V. Levadny and M. Yamazaki, *Langmuir*, 2015, **31**, 3391-3401.
25. E. Evans, V. Heinrich, F. Ludwig and W. Rawicz, *Biophys. J.*, 2003, **85**, 2342-2350.
26. E. Evans and B. A. Smith, *New J. Phys.*, 2011, **13**, 095010.
27. V. Levadny, T. Tsuboi, M. Belaya and M. Yamazaki, *Langmuir*, 2013, **29**, 3848-3852.
28. M. A. S. Karal, V. Levadny, T. Tsuboi, M. Belaya and M. Yamazaki, *Phys. Rev. E*, 2015, **92**, 012708.
29. M. K. Sarkar, M. A. S. Karal, M. Ahmed, M. K. Ahamed, S. Ahammed, S. Sharmin and S. U. A. Shibly, *Plos One*, 2021, **16**, e0251690.
30. F. Brochard-Wyart, P. -G. De Gennes and O. Sandre, *Physica A*, 2000, **278**, 32-51.
31. R. Ryham, I. Berezovik and F. S. Cohen, *Biophys. J.*, 2011, **101**, 2929-2938.
32. M. M. Or Rashid, M. M. R. Moghal, M. M. Billah, M. Hasan and M. Yamazaki, *BBA-Biomembranes*, ***2020***, **1862**, 183381.
33. Y. Tamba, H. Terashima and M. Yamazaki, *Chem. Phys. Lipids*, 2011, **164**, 351-358.
34. W. Rawicz, K. C. Olbrich, T. McIntosh, D. Needham and E. Evans, *Biophys. J.*, 2000, **79**, 328-339.
35. E. A. Evans, R. Waugh and L. Melnik, *Biophys. J.***,** 1976, **16**, 585-595.
36. Y. Tamba, S. Ohba, M. Kubota, H. Yoshioka, H. Yoshioka and M. Yamazaki, *Biophys. J.*, 2007, **92**, 3178-3194.

37. F. Hossain, M. M. R. Moghal, M. Z. Islam, M. Moniruzzaman and M. Yamazaki, *J. Biol. Chem*., 2019, **294**, 10449-10462.
38. O. Sandre, L. Moreaux and F. Brochard-Wyart, *Proc. Natl. Acad. Sci. USA*.**,** 1999, **96**, 10591-10596.
39. E. Karatekin, O. Sandre, H. Guitouni, N. Borghi, P. –H. Puech and F. Brochard-Wyart, *Biophys. J.*, 2003, **84**, 1734-1749.
40. B. Bechiniger, M. Zasloff and S. J. Opella, *Protein. Sci.*, 1993, **2**, 2077-2084.
41. E. Strandberg, P. Tremouihac, P. Wadhwani and A. S. Ulrich, *BBA-Biomembranes*, 2009, **1788**, 1667-1679.
42. W. C. Wimley and S. H. White, *Nat. Struct. Biol.*, 1996, 3, 842-848.
43. V. Levadnyy, M. Hasan, S. K. Saha and M. Yamazaki, *J. Phys*. *Chem. B*, 2019, **123**, 4645-4652.
44. M. Hasan, M. A. S. Karal, V. Levadnyy and M. Yamazaki, *Langmuir***,** 2018, **34**, 3349-3362.
45. F. Parvez, J. M. Alam, H. Dohra and M. Yamazaki, *BBA-Biomembrane*, 2018, **1860**, 2262-2271.
46. H. W. Huang, F.-Y. Chen and M. -T. Lee, *Phys. Rev. Lett.*, 2004, **92**, 198304.
47. J. D. Litster, *Phys. Lett. A*, 1975, **53**, 193- 194.
48. R. W. Glaser, S. L. Leikin, L. V. Chernomordik, V. F. Pastushenko and A. I. Sokirko, *Biochim. Biophys. Acta*, 1988, **940,** 275-287.
49. G. Fuertes, D. Giménez, S. Esteban-Martín, O. L. Sánchez-Muñoz and J. Salgado, *Eur. Biophys. J.,* 2011, **40**, 399-415.
50. D. P. Tieleman, H. Leontiadou, A. E. Mark and S. -J. Marrink, *J. Amer. Chem. Soc.*, 2003, **125**, 6382-6383.
51. T. V. Tolpekina, W. K. den Otter and W. J. Briels, *J. Chem. Phys.*, 2004, **121**, 12060-12066.
52. J. Wohlert, W. K. den Otter, O. Edholm and W. J. Briels, *J. Chem. Phys.*, 2006, **124**, 154905.
53. S. A. Akimov, P. E. Volynsky, T. R. Galimzyanov, P. I. Kuzmin, K. V. Pavlov and O. V. Batishchev, *Sci. Rep*., 2017, 7, 12509.
54. M. A. S. Karal, V. Levadnyy and M. Yamazaki, *Phys. Chem. Chem. Phys*., 2016, **18**, 13487-13495.
55. Y. Tamba, H. Ariyama, V. Levadny and M. Yamazaki, *J. Phys. Chem. B*., 2010, **114**, 12018-12026.
56. L. T. Yang, M. Weiss, R. I. Lehrer and H. W. Huang, *Biophys. J.*, 2000, **79**, 2002-2009.
57. P.-G. De Gennes, F. Brochard-Wyart and D. Quere, *Capillarity and wetting phenomena; Drops, bubbles, pearls, waves*, Springer, New York, 2004.
58. T. M. Domingues, K. A. Riske and A. Milanda, *Langmuir*, 2010, **26**, 11077-11084.
59. M. P. Dos Santos Cabrera, D. S. Alvares, N. B. Leite, B. M. de Souza, M. S. Palma, K. A. Riske and J. R. Neto, *Langmuir*, 2011, **27**, 10805-10813.
60. Y. Pouny, D. Rapaport, A. Mor, P. Nicolas and Y. Shai, *Biochemistry*, 1992, **51**, 12416-12423.
61. M. Z. Islam, S. Sharmin, V. Levadnyy, S. U. A. Shibly and M. Yamazaki, *Langmuir*, 2017, **33**, 2433-2443.

Table 1

(A) Interaction of 5.8 μM Mag

ΔC^0 (mOsm/L)	σ_{in} (Π) (mN/m)	δ_{eq}	δ_{eq} (ΔC^0)/δ_{eq} (0)	σ_{in} (Mag) (mN/m)	σ_{in} (total) (mN/m)
0	0	0.031	1	2.2	2.2
5	0.6	0.027	0.87	1.9	2.5
12	1.3	0.020	0.65	1.4	2.7

(B) Interaction of 20 μM Mag.

ΔC^0 (mOsm/L)	σ_{in} (Π) (mN/m)	δ_{eq}	σ_{in} (Mag) (mN/m)	σ_{in} (total) (mN/m)
0	0	0.041	2.9	2.9
5	0.6	0.036 (= 0.041 × 0.87)	2.5	3.1
12	1.3	0.027 (= 0.041 × 0.65)	1.9	3.2

Table 1 Mag-induced fractional area change of the GUV membrane under osmotic pressure at the binding equilibrium, δ_{eq}, the tension in the inner leaflet due to Π (σ_{in} (Π)), the tension in the inner leaflet due to the binding of Mag in the outer leaflet (σ_{in} (Mag)), and the total tension in the inner leaflet (σ_{in} (total)). (A) Interaction of 5.8 μM Mag. The values of δ_{eq} were obtained from Fig. 5C. (B) Interaction of 20 μM Mag.

Figure 1

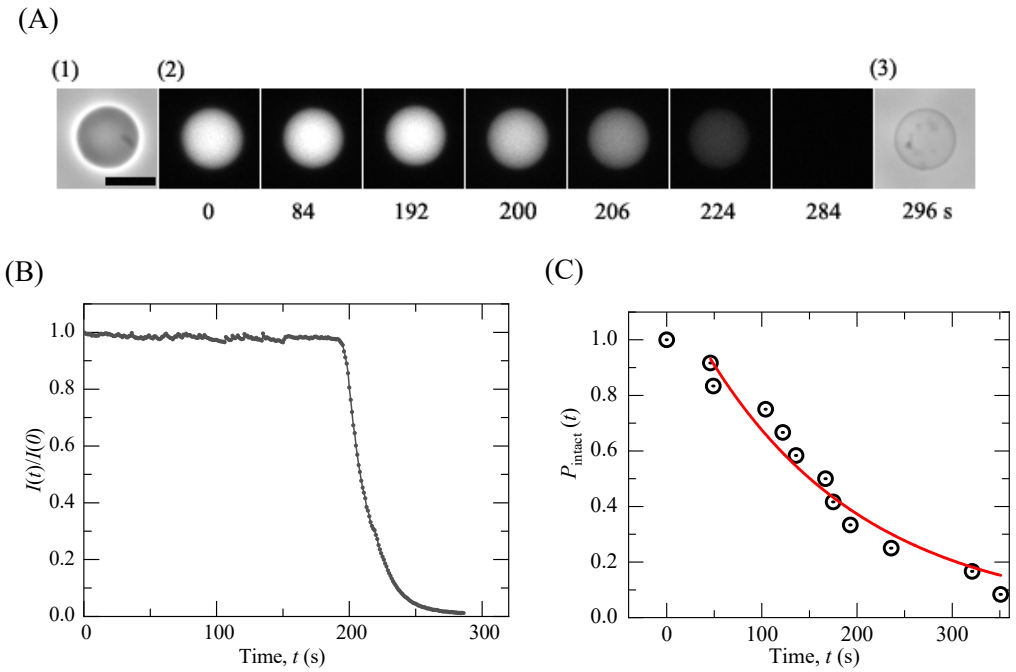

Figure 1: Mag-induced (nanometer-scale) pore formation in GUVs under an osmotic pressure due to $\Delta C^0 = 5$ mOsm/L. (A) Interaction of 20 μM Mag with a single DOPG/DOPC (4/6) -GUV containing AF488. (1) and (3) show the phase contrast images and (2) shows fluorescence images due to AF488 in the GUV lumen. The interaction time is denoted by the number below each image. Bar, 20 μm. (B) Time course of change in the normalized intensity, $I(t)/I(0)$, of AF488 fluorescence of the GUV lumen shown in the panel A. (C) Time course of change in the fraction of the intact GUV among all the examined GUVs ($n = 12$), P_{intact}, of single GUVs. The red line represents the best fit curve of Eq. 4.

Figure 2

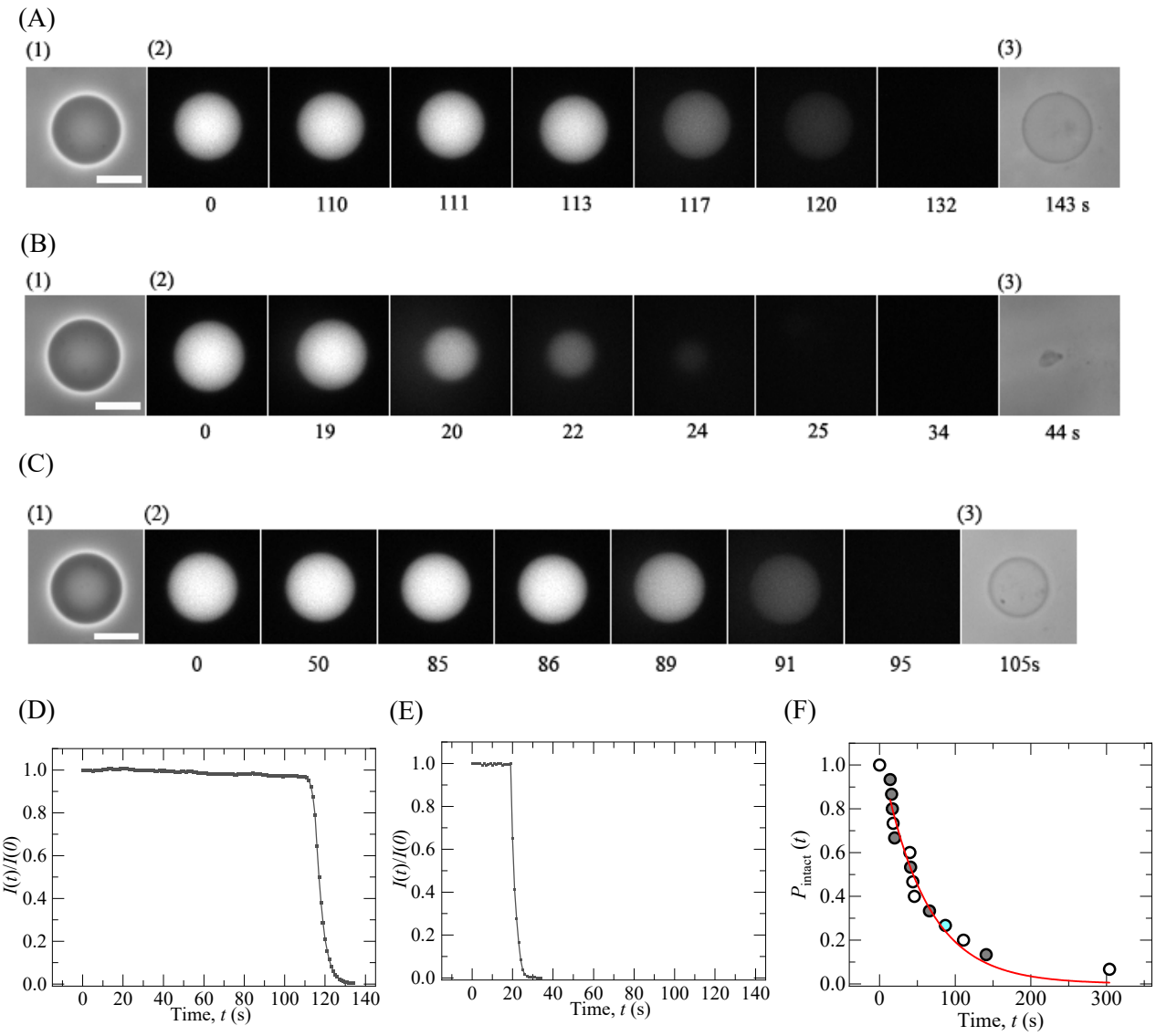

Figure 2: Various types of Mag-induced leakage in GUVs under an osmotic pressure due to ΔC^0 = 12 mOsm/L. (A) Leakage without rupture (through nanometer-scale pores), (B) complete rupture, and (C) transient rupture. Interaction of 20 μM Mag with a single DOPG/DOPC (4/6)-GUV containing AF488. (1) and (3) show the phase contrast images and (2) shows fluorescence images due to AF488 in the GUV lumen. The interaction time is denoted by the number below each image. Bar, 20 μm. (D) and (E) are time courses of change in the normalized intensity, $I(t)/I(0)$, of AF488 fluorescence of the GUV lumen shown in the panel A and B, respectively. (F) Time course of change in the fraction of the intact GUV (P_{intact}) among all the examined GUVs (n = 15 including three types of results, i.e., leakage without rupture (○), complete rupture (grey ●), and transient rupture (cyan ●)). The red line represents the best fit curve of Eq. 4.

Figure 3

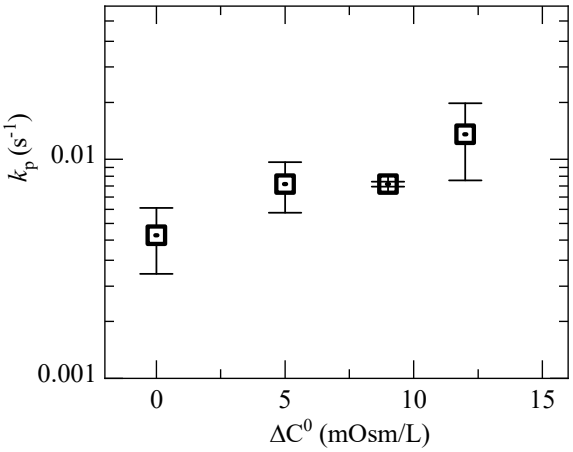

Figure 3: Effect of osmotic pressure due to ΔC^0 on the rate constant of Mag-induced pore formation, k_p. The points represent mean values and error bars correspond to ± SD values (N = 3–4).

Figure 4

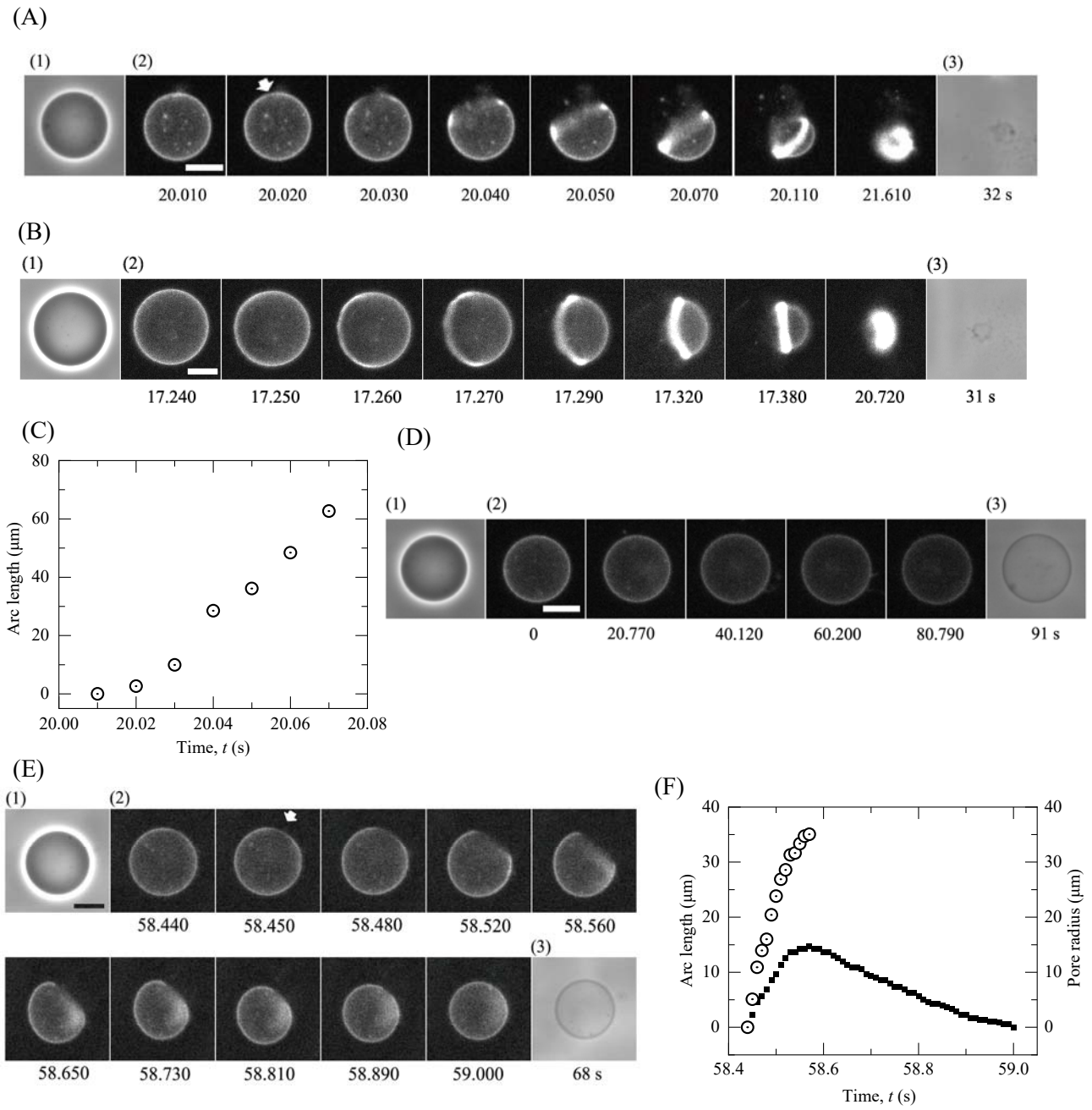

Figure 4: Shape change of GUVs during pore formation induced by Mag. (A) and (B) show two cases of growing micrometer-scale pores ending up with complete GUV rupture. (D) shows leakage through a nanopore (not visible) without vesicle rupture, and (E) shows a case with a visible but transient micrometer pore (i.e., transient rupture). Interaction of 20 μM Mag with a single DOPG/DOPC/NBD-PE (39/60/1)-GUV in the presence of osmotic pressure due to ΔC^0 = 12 mOsm/L. (1) and (3) show the phase contrast images and (2) shows fluorescence images due to NBD-PE in the GUV membrane. The interaction time is denoted by the number below each image. Bar, 20 μm. (C) Time course of change in arc length of the dark spot of the membrane (i.e., micrometer-scale pore) shown in panel A. (F) Time course of change in arc length of the dark spot of the membrane (○) and in pore radius (■) shown in the panel E.

Figure 5

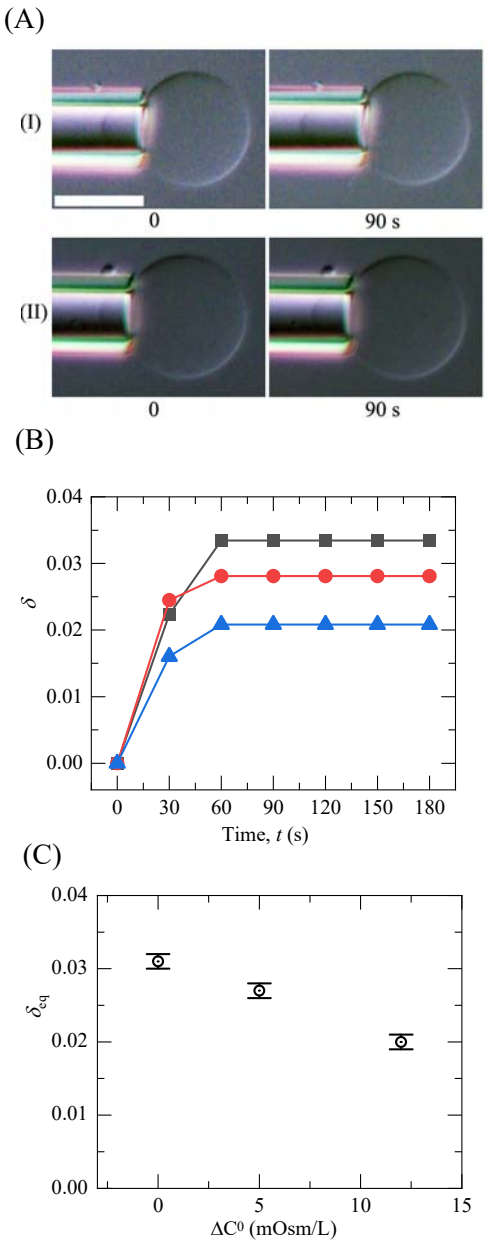

Figure 5: Effect of osmotic pressure on the Mag-induced area change of GUVs. (A) Interaction of 5.8 μM Mag with single DOPG/DOPC (4/6)-GUVs in (I) the absence of osmotic pressure (ΔC^0 = 0 mOsm/L) and (II) the presence of osmotic pressure due to ΔC^0 =12 mOsm/L. The images of the GUVs before the interaction (0 s) and after the interaction of Mag for 90 s are shown. The increment of the projection length after 90 s interaction in the absence of osmotic pressure (I) is larger than that in the presence of ΔC^0 = 12 mOsm/L (II). Bar, 20 μm. (B) Time course of the fractional area change of the GUV (δ) during its interaction with 5.8 μM Mag. (■) ΔC^0 = 0 mOsm/L (i.e., isotonic condition), (red ●) ΔC^0 = 5 mOsm/L, and (blue ▲) ΔC^0 = 12 mOsm/L. (C) Effect of osmotic pressure on the equilibrium value of the fractional area change of the GUV (δ_{eq}) induced by Mag. The error bars indicate the standard error of δ_{eq}.

Figure 6

(A)

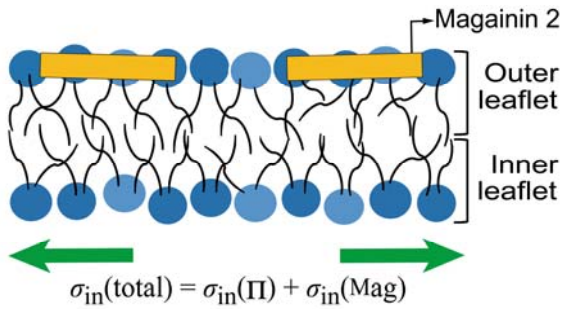

(B)

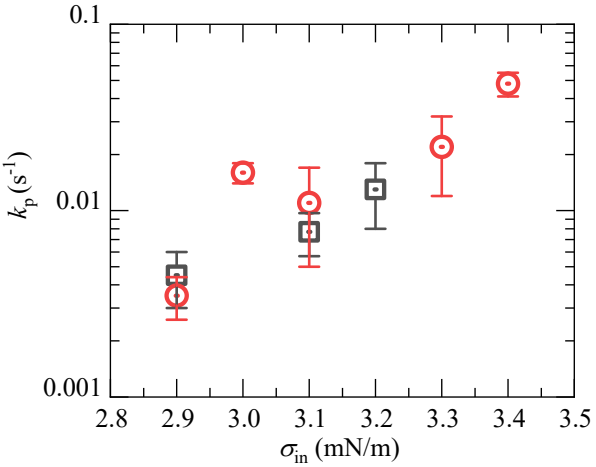

Figure 6: The role of the membrane tension in the inner leaflet of a GUV in the Mag-induced pore formation. (A) A scheme of the total membrane tension in the inner leaflet, σ_{in} (total), induced by the osmotic pressure (σ_{in} (Π)) and the binding of Mag to the outer leaflet (σ_{in} (Mag)). (B) The relationship between the total membrane tension in the inner leaflet, σ_{in} (total), and the rate constant of Mag-induced pore formation, k_p. (□) Interaction of 20 μM Mag with single GUVs under various osmotic pressures, (red ○) Interaction of various concentrations of Mag with single GUVs in the absence of osmotic pressure (24).

Figure 7

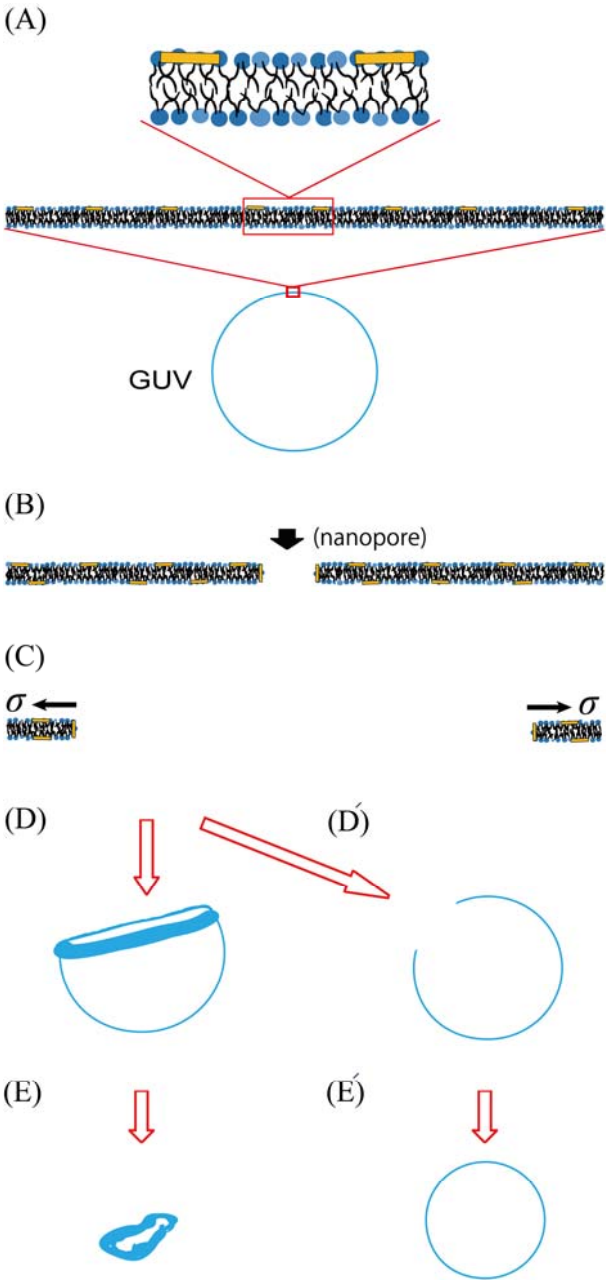

Figure 7: A hypothesis on the evolution of the Mag-induced nanometer-scale pore to the complete rupture and transient rupture of a GUV and its mechanism. (A) Mag binds to the membrane interface of the outer leaflet of a GUV. A Mag molecule is denoted by an orange rectangle. (B) Mag induces a nanometer-scale pore (i.e., nanopore) in the GUV membrane. In this pore, the line tension of the pore rim is small due to the presence of Mag at the pore rim, which stabilizes the toroidal pore. (C) A residual membrane tension due to Π, σ, increases the pore size to produce a micrometer-scale pore observable using optical microscopy. From this stage, there are two routes. One route is for the complete rupture (→ D→ E). (D) The folding of membranes occurs at the rim of a micrometer-scale pore. (E) The pore size increases further with time to form a small aggregate of lipid membranes. The other route is for the transient rupture (→ D′→ E′). (D′) The folding of membranes does not occur at the rim of a micrometer-scale pore. (E′) Due to the line tension the pore is closed, which produces the GUV with a smaller diameter.

TOC Graphic

Effect of Osmotic Pressure on Pore Formation in Lipid bilayers by the Antimicrobial Peptide Magainin 2

Md. Masum Billah, Samiron Kumar Saha, Md. Mamun Or Rashid, Farzana Hossain, and Masahito Yamazaki